Article publicat / *Published paper*:

Bermudez, Carlos; [et al.]. Stent optical inspection system calibration and performance. "Applied optics", Marzo 2017, vol. 56(9), p. 134-141

DOI: 10.1364/AO.56.00D134

Stent Optical Inspection System calibration and performance

Carlos Bermudez[1,2,*], Ferran Laguarta[1], Cristina Cadevall[1,2], Aitor Matilla[2], Sergi Ibañez[3], Roger Artigas[1,2]

[1]*Center for Sensors, Instruments and Systems Development (CD6), Technical University of Catalonia (UPC), Rambla Sant Nebridi 10, E-08222 Terrassa, Spain*
[2]*Sensofar-Tech, S.L., Parc Audiovisual de Catalunya, Ctra. BV1274 km 1, E-08225 Terrassa, Spain*
[3]*Sensofar-Medical, S.L., Parc Audiovisual de Catalunya, Ctra. BV1274 km 1, E-08225 Terrassa, Spain*
**Corresponding author: bermudez@sensofar.com*

Implantable medical devices, such as stents, have to be inspected 100% so no defective one is implanted into a human body. In this paper, a novel optical stent inspection system is presented. By the combination of a high numerical aperture microscope, a triple illumination system, a rotational stage, and a CMOS camera, unrolled sections of the outer and inner surfaces of the stent are obtained with high resolution at high speed with a line-scan approach. In this paper, a comparison between the conventional microscope image formation and this new approach is shown. A calibration process, and the investigation of the error sources that lead to inaccuracies of the critical dimensions measurements are presented.

OCIS codes: *(110.0180) Microscopy; (120.3930) Metrological instrumentation; (120.3940) Metrology; (120.4630) Optical inspection.*

http://dx.doi.org/10.1364/AO.99.099999

1. INTRODUCTION

In recent times, stent manufacturing has grown exponentially. Stents are miniature hollow cylinders that are implanted into the human body in order to remove a stenotic lesion or to facilitate access for surgery. They are manufactured from raw tubes, which are laser-cut. Some of the most important processes during the manufacturing of a stent are dimensional control and visual inspection. Defects and shape deviations from the nominal design are affecting its performance, lifetime, and even cause a hazard to the patient. Stent quality assurance processes are tremendously strict. Inspection of a stent is today an extremely labor-intensive, time-consuming and expensive process, executed visually by skilled operators equipped with optical microscopes. Human errors can eventually yield samples out of specifications, and increase the stent rejection, which ends with higher manufacturing costs.

Few automated inspection systems (using contact and non-contact techniques) have been proposed in the recent years to provide objectivity, repeatability and speed to the inspection process. One of the first developments is based on a stent inserted onto a mandrel, which is rotating, illuminated with a backlight and imaged with a line-scan camera [1]. Another approach to avoid some of the limitations of the mandrel is the use of two rollers with dual illumination [2]. However, those systems are using telecentric optics to form the image of the surface of the stent, using low numerical aperture, and thus recovering images with low resolution [3]. Another disadvantage is that they don't measure the inner surface of the stent.

In this paper a new optical, high resolution inspection system is presented. Our approach uses a high numerical aperture imaging optics, a triple-light illumination arrangement (epi-illumination, back and side) a CMOS camera, and a high-precision rotational stage aimed to obtain unrolled images of all stent surfaces [4]. We provide well focused and high contrast images of the outer, inner and side surfaces with up to 1µm lateral resolution. The obtained images are used for measuring strut dimensions, roundness quality of the edges after the polishing stage, and also for detection and classification of defects.

2. EXPERIMENTAL SETUP

In order to perform accurate stent dimensional metrology it is essential to acquire well focused and high contrast images. To acquire such images we have implemented the following approach: a microscope arrangement with the use of high numerial aperture optics, a triple illumination system, a CMOS camera that can behave as both area and line scan, and a high-precision rotational stage. In a bright field microscope, the image of stent-like samples decreases in light gathering and focus for those regions far from the apex (Figure 1a). With the line scan mode of the camera and the rotational stage rotating at a continuous speed, we compose the image acquiring data from the apex of the stent (Figure 1b).

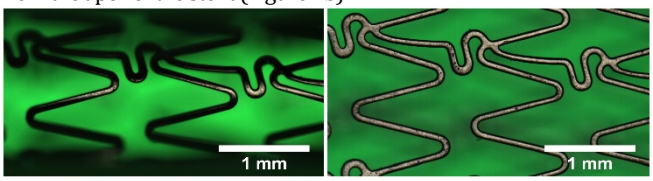

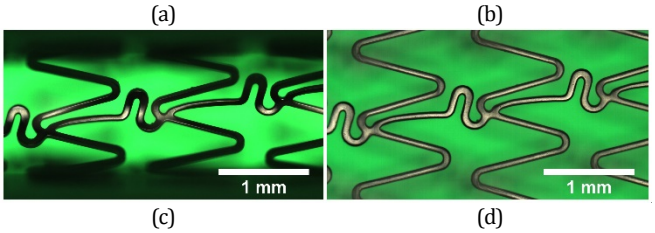

Fig. 1. Images taken with a 5X 0.15NA lens. Outer surface: (a) bright field screenshot, (b) part of a line-scan acquired section. Inner surface: (c) bright field screenshot, (d) part of a line-scan acquired section.

Figure 2 shows the optical and mechanical arrangement of our approach. A white light LED illuminates the field diaphragm of a microscope and is imaged onto the entrance pupil of a microscope objective in a Köhler type illumination scheme. The light reflected from the stent surface is going back to the objective, which is forming an image onto an area scan camera. Two additional light sources are located at one side and under the roller stage to provide diffuse back and side illumination, being the latter intended to facilitate the visual inspection to the user and for further investigation related to stent sidewalls imaging. The resulting image can be seen in Figure 1a. With the use of a motorized nosepiece, we used microscope objective magnifications ranging from 2.5X to 20X with numerical apertures from 0.075 to 0.45. This provides the possibility to acquire images with a very large field of view (FOV) (2.5X: 7.20mm horizontal, 3.52µm lateral resolution) while keeping an optical resolution below 1µm (20X: 0.9mm horizontal FOV, 0.44µm lateral resolution).

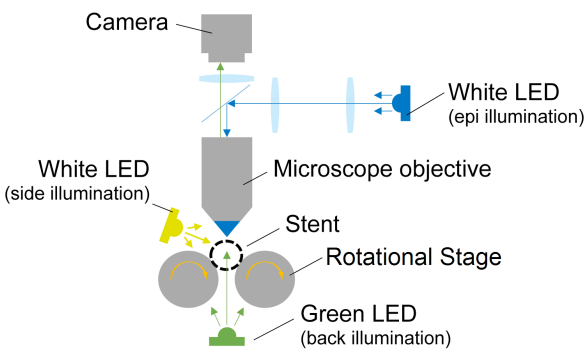

Fig. 2. Triple illumination system arrangement.

The camera used in this study is capable to acquire with an area scan mode (2 million pixel) or line scan (2048 pixels) at much higher frequency. Unrolled images as shown in Figure 1b is obtained with the line scan mode of the camera and the rotational stage rotating at continuous speed. The rotational stage is a two-roller arrangement consisting of two stainless steel nuclei rollers enclosed with a white polyoxymethylene (POM) 2mm thick cover to provide enough stiffness and a smooth surface (Ra < 0,8µm). Light reflections are avoided thanks to the elevated diffusion capacity of the plastic. Roller diameter and distance between them is optimized to maintain enough back light aperture while providing the possibility to focus short working distances objectives, such as a 20X 0.45NA with a working distance of 4.5mm, and at the same time able to focus in the inner surface of stents ranging from 1.5mm to 15mm in outer diameter (OD) without being limited by the rollers.

3. CRITICAL DIMENSIONS

The most common dimensional analysis in stent inspection are strut width and edge roundness .We use segmentation algorithms to isolate stent struts from the background. We obtain binary masks from strut outer geometry of Figure 3a, and edges geometry with the use of morphological operations and a blob detection algorithm(Figure 3b and 3c). From the original image and said binary masks, critical dimension analysis, defect detection and classification and further 3D metrology investigation can be performed.

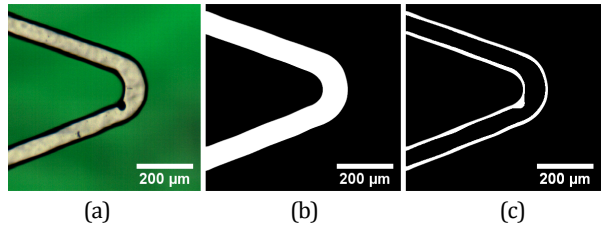

Fig. 3. Stent with a crack defect, (a) unrolled image, (b) surface mask, (c) edge mask.

A. Critical dimensions measurement

We have analyzed the differences when measuring critical dimensions with a conventional microscope in comparison to our unrolled images. Conventional microscope images measure the projected surface width, while unrolled images measure the arc section of the strut. The result is a larger measurement, which fits exactly to the nominal design, but not to what the inspection operators are used to measure. In Figure 4, a stent section is shown. Strut width *CD* can be defined as a function of the stent outer diameter *D*, the roundness radius *r* of the edge, and the angle formed by its walls with the observation axis, *θ*.

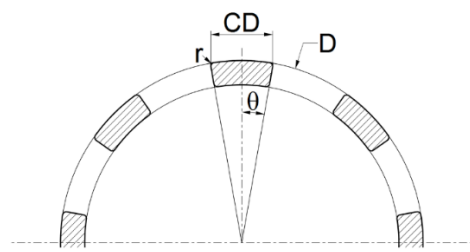

Fig. 4. Section of a stent strut.

Assuming the strut does not have rounded edges, that is, without surface treatment, its critical dimension in a conventional microscope may be described as:

$$CD_M = 2\left(\frac{D}{2}\sin(\theta)\right) \quad \textbf{(1)}$$

The factor of 2 takes into account that *θ* corresponds to one half of the strut while in an unrolled image the critical dimension corresponds to two times the arc length:

$$CD_U = 2\left(\frac{D}{2}\theta\right) \quad \textbf{(2)}$$

Surface treatment has an effect on the critical dimensions measurements due to the modification of the stent edge geometry. Figure 5 shows the difference between a non-treated, sharp-edge strut Figure 5a versus its geometry after surface treatment Figure 5b, being CD_M' the critical dimension measured with the microscope with rounded edges.

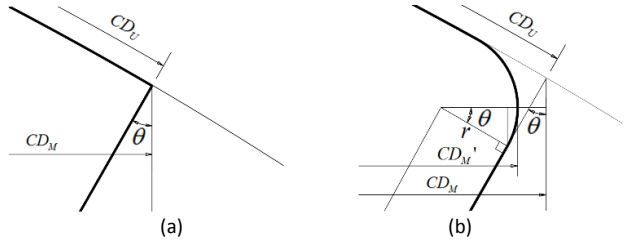

Fig. 5. Zoom view of a strut edge, (a) without surface treatment, (b) with surface treatment

This critical dimension CD_M' is determined by:

$$CD_M' = 2\left(\sin(\theta)\sqrt{\frac{D^2}{4} - Dr} + r(1-\cos(\theta))\right)\Bigg|_{\theta>\theta_{MIN}} \quad (3)$$

Where r is the radius of the edge roundness. This expression is only valid for a certain interval, $\theta>\theta_{MIN}$, which stands for the limit where roundness diameter equals to strut thickness, and meaning that smaller struts have no sense. Figure 6 shows the relatioship of this limitation between stent diameter and edge roundness radius.

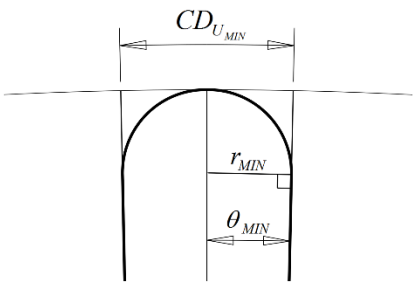

Fig. 6. Minimum strut width is determined by the roundness radius

The minimum angle θ_{MIN} can be obtained through:

$$\theta_{MIN} > \arcsin\left(\frac{r_{MIN}}{D/2 - r_{MIN}}\right) \quad (4)$$

And by substituing (4) in (2), the minimum strut width CD_{Umin} is defined as:

$$CD_{U\min} > D\arcsin\left(\frac{r}{D/2 - r}\right) \quad (5)$$

Therefore, by substituting (3) in (2) taking into account the condition (5), we obtain that the critical dimension of a stent with rounded edges measured with a microscope is the following:

$$CD_M' = 2\left(\sin\left(\frac{CD_U}{D}\right)\sqrt{\frac{D^2}{4} - Dr} + r\left(1-\cos\left(\frac{CD_U}{D}\right)\right)\right)\Bigg|_{CD_U > CD_{U\,MIN}} \quad (6)$$

We can assert that the ratio between a measurement in a conventional microscope versus one in an unrolled image is dependent on edge roundness, and the difererence between them is increasing together with the strut width. Figure 7 shows the ratio between CD_M' and CD_U, versus the strut width CD_U for a stent with outer diameter of 1.5mm and with different edge roundness:

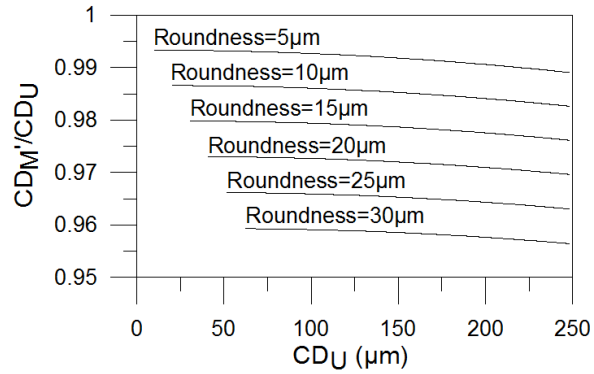

Fig. 7. Critical dimension measurement ratio between a conventional microscope image and an unrolled acquisition, for 6 given strut edge roundness values of a 1.5mm outer diameter stent.

We have checked this behavior with an electropolished 1.5mm diameter stent with 30µm roundness radius. Two profile cuts have been obtained at the same stent location (Figure 8) and the measurement of such profiles shows a strut width of 97.1µm in the screenshot (conventional microscope image) versus 101.0µm corresponding to the unrolled image, revealing a measurement ratio CD_M'/CD_U of 0.96.

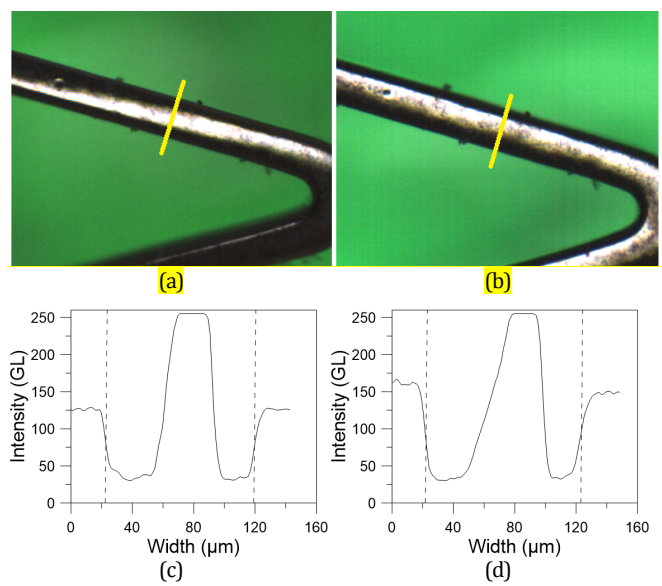

Fig. 8. Critical dimension measurement comparison between (a) a conventional microscope screenshot and (b) an unrolled acquisition. Width results are 97.1µm for the screenshot profile (c) and 101µm for the unrolled acquisition profile (d).

4. CALIBRATION

Critical dimension measurement accuracy is achieved through a calibration process of the complete setup. This process consists of precise alignment of the roller stage with the optical axis, calibration of the optical system magnification and rotational speed, adjusting the parfocal and parcentric objective offsets and fine-tuning the camera acquisition time to avoid aliasing with the illumination frequency switching. Being no commercialy avaliable specimen for the magnification calibration in the unrolled direction, we have manufactured ourselves a new, state of the art, calibration specimen for unrolled image acquisition.

A. Roller stage and stent position

To ensure the proper focusing of the microscope objective onto the surface, the geometry and positioning of the rollers with respect to the optical axis has to be calibrated.

It is important to note that this calibration procedure has to be performed with one single objective, in our case a 5X magnification objective, because different parfocality and parcentricity errors appear between objectives, as will be seen in subsection 4.C.

The first step is to know exactly the central position between the two rollers in the Y direction (transversal to the stent), where the stent will be placed. X position (longitudinal to the stent axis) is irrelevant in this step. This is done by acquiring one image around the central region where the back illumination should be centered. Although rollers are out of focus (Figure 9a), the sum of all the image columns (dashed line in Figure 9b) allows detecting the center between them. In our case we apply a Savitzky-Golay derivative with a 9-point window size to detect the edge transition (solid line in Figure 9b).

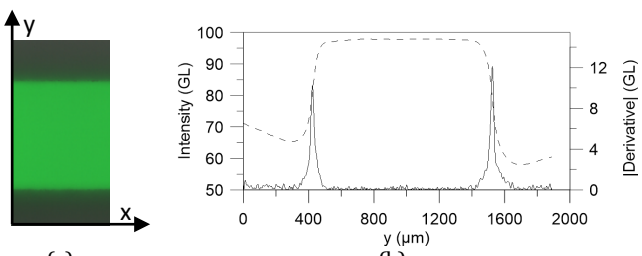

(a) (b)

Fig. 9. (a) Back side illumination enabled, focusing the rollers edges, (b) filtered mean profile (dashed line) and its derivative (modulus, solid line).

Once the derivative of the average intensity profile is obtained, a peak detection algorithm is applied around the peaks with a parabolic fitting. This provides subpixel accuracy, meaning less than 1 micron positioning resolution. If the result value is not aligned with the optical axis, the corresponding offset to the Y stage is automatically applied. The algorithm runs again to compensate a slight deviation that may be remaining due to the effect of back light projection and numerical aperture.

The next calibration step is to find the rollers Z height. First, Y stage is moved a distance corresponding to half the separation between the two rollers axes, in our case 5.95mm, and the Z stage to the height where the apex of the roller is located. This value is known by design.

At this point, an autofocus algorithm is carried out, which finds the highest contrast plane using an image processing algorithm that looks for the image variance, taking advance of the roller surface irregularities.

Afterwards, the Y stage is moved to the second roller apex to find its height with the same procedure. The average of the two apex heights determines the rollers average height at the optical axis. If the two heights are different, a skewness error appears. This skewness makes found Z value only valid for a range of stent diameters whose apex is near the one of the rollers, as it will be seen in next chapter.

Once the Y stage is aligned with the optical axis and the Z position of rollers apex is known, the position of any stent outer diameter can be obtained by simple geometrical calculations, as can be observed in Figure 10:

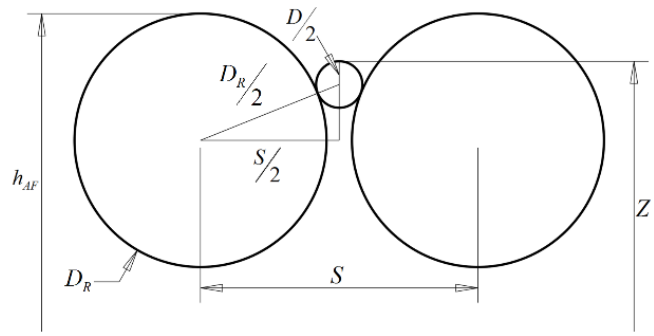

Fig. 10. Outer diameter Z position determining.

Finally, the height of the stent apex Z is determined by:

$$Z = h_{AF} - \frac{D_R}{2} + \sqrt{\left(\frac{D_R}{2} + \frac{D}{2}\right)^2 - \frac{S^2}{4}} + \frac{D}{2} \qquad \textbf{(7)}$$

Where D_R stands for the roller diameter, S is the separation between the two rollers axes, D is the stent diameter, and h_{AF} the height of the rollers apex determined by the autofocus algorithm.

B. Optical magnification

The real optical magnification of the microscope objective is calibrated with a magnification calibration specimen for microscopes in the X direction. The unrolled direction magnification is dependent on the acquisition framerate and the rotational speed. We developed a custom calibration specimen to calibrate the rotational speed at a given, fixed framerate. The specimen consists of a chromium coated rod lens and laser-engraved Ronchi grating parallel to the radial direction, with 50µm pitch.

1. X magnification

The microscope real optical magnification is calibrated by a certified calibration specimen, in our case a 150mm long ruler with 10 µm TED PELLA model MR1 (Figure 11a). With the microscope objective, a 125mm tube lens and a camera with 5.5µm pixel size, we obtain a sampling as is depicted in Table 1:

Table 1 Optical sampling for different magnifications

Magnification	2.5X	5X	10X	20X	50X
Sampling (µm)	3.52	1.76	0.88	0.44	0.176

In order to calibrate the magnification, an algorithm extracts the intensity profile of the optical ruler around the marks (Figure 11b) and calculates the mean distance between them through the PS_m parameter (ISO 4287), which determines the average value of the elements spacing.

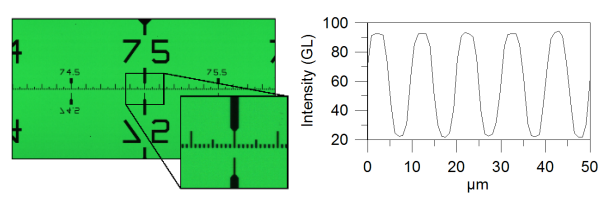

(a) (b)

Fig. 11. (a) 150mm, 10.0µm resolution optical ruler, (b) intensity profile at the center of the ruler.

Once the average width between the ruler marks is obtained, it is divided by the nominal value (10.0µm) to obtain the calibration factor. This procedure is repeated for every objective.

2. Rotation speed

Although the real optical magnification for a bright field image can be calibrated with an optical ruler, the magnification in Y direction of an unrolled image is given by two additional parameters: the camera framerate and the rotating speed. Acquisition framerate has to be fixed to a certain value in order not to cause aliasing with the illumination board switching frequency, as it will be seen in chapter 4.D. Therefore, the variable parameter is the rotating speed, that is also dependent on the magnification.

In our case, we have manufactured our own custom calibration specimen on a cylindrical lens of 5mmØx20mm, coated with a 300nm chromium film and laser engraved with a 50µm Ronchi grating. With the aim to have one single calibration specimen, we engraved two gratings in the transversal and in the axial direction (Figure 12), which allows us to do both calibrations.

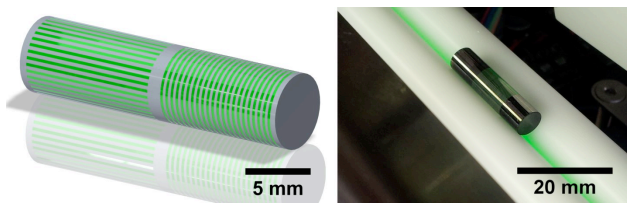

(a) (b)

Fig. 12. (a) 3D representation of the calibration specimen, (b) picture of the calibration rod, 5mmØx20mm.

Although the laser engraved lines have a nominal width of 25µm with a 50µm pitch, the real width has to be measured by an traceable calibrated instrument, which will yield the nominal value and the accumulated uncertainty.

The procedure to calibrate the rotating speed is very similar to the one depicted in chapter 4.B.1, but with the acquisition of an unrolled image (Figure 13). The obtained value PS_m has to be compared to the real PS_m of the specimen, and the factor is obtained by the division of the latter by the former one applied to the rotating speed.

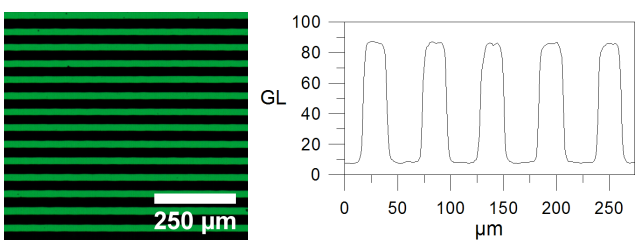

(a) (b)

Fig. 13. (a) Unrolled image of the calibration specimen, (b) average vertical light intensity profile.

C. Parfocal and parcentric offsets, and light efficiency between objectives

To obtain centered images with different objectives, parfocal and parcentric misalignments between them have to be adjusted. Additionally, every objective could have different light efficiency due to different numerical apertures. A light factor between them is calibrated to take this effect into account.

1. Parfocal and parcentric offset calibration

Due to microscope objective and nosepiece fabrication tolerances, the focal plane of an objective could be different from another objective, resulting in a parfocal error. Same would happen with the optical axis deviation, which would make the image to appear displaced laterally between two objectives. These two error can be compensated with an automatic XYZ adjustment. In our case we have defined a reference objective (5X magnification) to calibrate the rest. The procedure is manual: the user has to focus a small feature on a sample and center it in a certain region of the image. After changing the objective, he has to repeat the same process by actuating the XYZ controls. The offsets between the actual and former positions correspond to the parfocal and parcentric adjustment of the latter objective.

2. Light factor calibration

Objectives can have have different light efficiencies. To avoid adjusting light intensity in every objective change, we have assigned a light factor to each one. To adjust them, we start from a reference objective that has this factor set to 1. The process is automatic: a back light autolight is performed, the objective to calibrate is positioned and light is adjusted iteratively until gray level in the central region of the image is the same as with the reference objective.

Although this light factor works satisfactorily with the back light, behavior is different with the epi-illumination, since this light crosses the objective twice. We calibrate separately an epi light factor by focusing a sample.

D. Aliasing in high speed image acquisition

Aliasing may appear due to the coupling of framerate and illumination PWM switching frequency, which in our case is 15kHz, 12bit (4096 levels). Frame integration time has to be adjusted to minimize this effect. As can be seen in Figure 14a, a desynchronization between lighting and acquisition can lead to an uneven light intensity across the image, whereas a well-adjusted acquisition time makes this effect unnoticeable (Figure 14b).

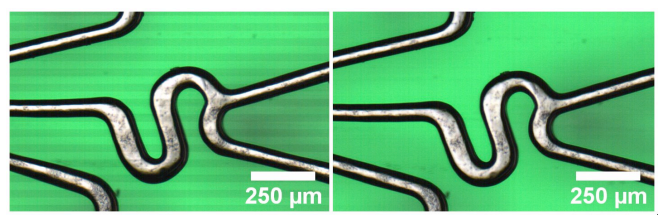

(a) (b)

Fig. 14. Unrolled image taken at 997fps, integration time of (a) 814µs, (b) 849s.

5. ERROR SOURCES

In order to accomplish the required image quality, the roller stage components require strict manufacturing tolerances. Small deviations of these parts are translated into focus errors, wrong magnification images, or even wrong positioning of the stent under the microscope. We have detected two types of errors that impose critical manufacturing tolerances: axis skewness and roller excentricity.

A. Axis skewness

When assembling the roller stage, the center-to-center line between the two rollers has to be perpendicular to the optical axis, and to the Z translation stage. If a skewness error is present between these two axes, different stents of different diameters will not focus onto its apex, but at a slightly lateral shift. To minimize this effect, we have established that the maximum angular error is the one that shifts the

apex between the smallest and largest stent diameter that the system can measure by 3 pixels of a 5X objective. In Figure 15, a zoom view of a roller stage section with a stent of outer 1.5mm outer diameter is shown.

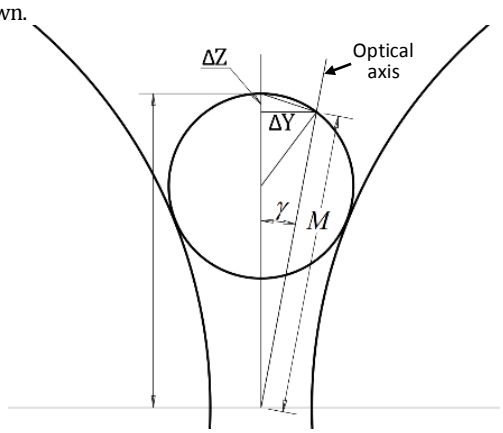

Fig. 15. Skewness error determination

To determine the Y and Z positioning errors (ΔY and ΔZ), first of all we determine the stent apex Z position (Z') with respect to the rollers center:

$$Z' = \frac{D}{2} + \sqrt{\left(\frac{D_R}{2} + \frac{D}{2}\right)^2 - \frac{S^2}{4}} \quad \textbf{(8)}$$

Where D/2 corresponds to the stent outer diameter, D_R to the roller diameter and S to the distance between the two rollers axes. Then, the distance M between the plane formed by the rollers axes and the stent surface along the Z skew axis is calculated through:

$$M = \left(Z' - \frac{D}{2}\right)\cos\gamma + \sqrt{\left(\left(Z' - \frac{D}{2}\right)\cos\gamma\right)^2 + DZ' - Z'^2} \quad \textbf{(9)}$$

Being γ the angle formed by the Z and the optical axes. Finally, we obtain the Y and Z positioning errors through:

$$\Delta Y = M \sin\gamma \quad \textbf{(10)}$$

$$\Delta Z = Z' - M\cos\gamma \quad \textbf{(11)}$$

Figure 16 shows the displacement in Y direction (ΔY) as a function of the skewness angle γ for three different stent outer diameters. A reference Y error limit has also been plotted, corresponding to 3 pixels error for a 5X lens:

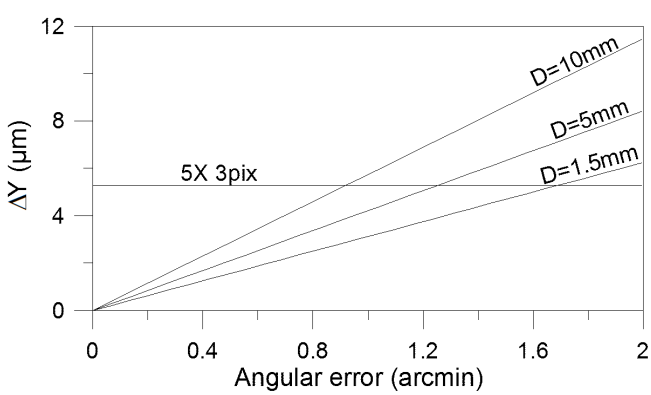

Fig. 16. Stent apex displacement in Y direction as a function of skewness.

As can be seen in the figure, maximum allowed skewness error is below 1arcmin, which means an extremelly tight manufacturing tolerance. To reduce such tolerance, we have caracterized this error by measuring the apex Y position of three different glass rods with diameters of 2mm, 5mm, and 10 mm. This characterization opens the possibility to shift the Y stage when loading a new stent into its correct position.

As regards to the error in the Z direction, Figure 17 shows that the error remains below 12µm for skewnesses under 1.6 arcmin. The maximum allowed error corresponding to the 5X 0.15NA lens depth of field (DoF), is 12.33µm for a λ=555nm.

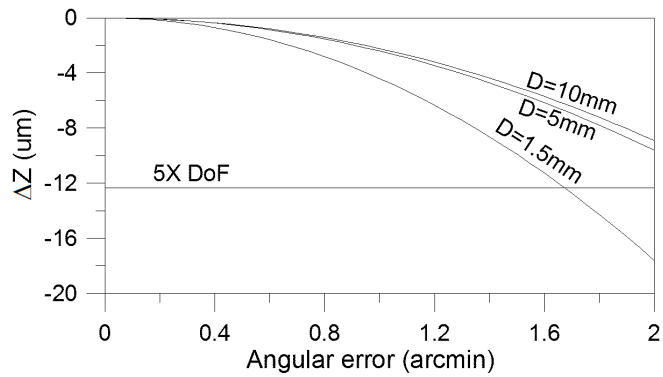

Fig. 17. Stent apex displacement in Z direction as a function of skewness.

B. Roller run-out

Each roller could have form deviations from the nominal cylindrical shape, and its rotational axis to be not totally parallel. During roller revolution, these deviations mean that the rollers locally separate or approach each other, making the stent to shift laterally and out of focus. We have established that the maximum excentricity error allowed is the one that keeps the stent within the depth of field of the objective and a maximum of 3 pixels shift.

Figure 18 shows a zoom view of the roller stage with one excentric roller:

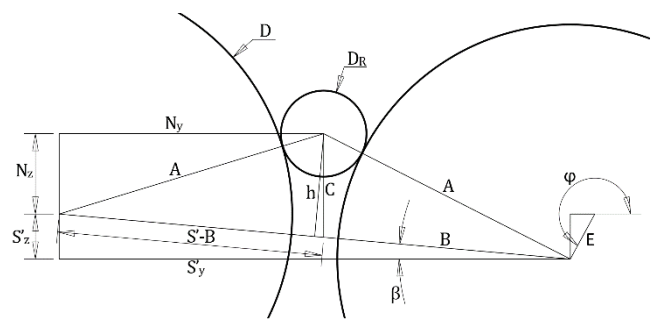

Fig. 18. Excentricity error determination

Stent position is determined with N_y and N_z, that are referenced to the non-excentric roller on the left. Excentricity effect is determined by the following equations:

$$S'_x = S + E\cos\varphi \quad \textbf{(12)}$$

$$S'_y = E\sin\varphi \quad \textbf{(13)}$$

$$\beta = \tan\left(\frac{S'_y}{S'_z}\right) \quad \textbf{(14)}$$

$$S' = \sqrt{S'^2_y + S'^2_z} \quad \textbf{(15)}$$

Where E is the constant, construction-defined excentricity error, S the roller axes theoretical separation, S' the real separation, which changes with the rotation angle φ, and β the angle formed by the two rollers axes and the horizontal plane. To reach the stent dynamic position, some intermediate variables (h, B and C) have to be described:

$$A^2 = \left(\frac{S'^2}{2}\right) + h^2 \quad \textbf{(16)}$$

Being A the sum of the radii of the roller and the stent ($D_R/2 + D/2$). B and C are obtained through:

$$C = \sqrt{\frac{\left(A^2 - \frac{S'^2}{4}\right)}{1 - \cos^2\left(\frac{\pi}{2} - \beta\right)}} \quad \textbf{(17)}$$

$$B = \frac{S}{2} + C\cos\left(\frac{\pi}{2} - \beta\right) \quad \textbf{(18)}$$

Finally, the stent position with respect to the stationary roller is determined by:

$$N_Y = (S' - B)\cos\beta \quad \textbf{(19)}$$

$$N_Z = C - (S' - B)\sin\beta \quad \textbf{(20)}$$

Both functions represent sinusoidal curves with different amplitudes, phases and offsets. Maximum errors are defined by these amplitudes or the peak to valley value. As regards to the Y displacement, which has minima and maxima at rotation angle φ depending on the stent diameter, we have calculated numerically the angles where the maxima condition is met using the derivative, and its displacement value:

$$PV_Y = N_{Y\,MAX} - N_{Y\,MIN} \quad \textbf{(21)}$$

As a result, Figure 19 shows the maximum Y error as a function of excentricity error, for three different stent diameters. The greater the stent diameter, the bigger the error due to the amplification effect of the stent apex distance to the stent-roller contact points.

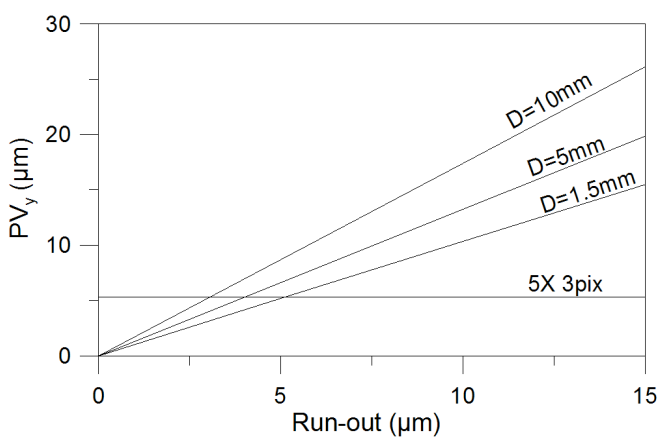

Fig. 19. Excentricity Y projection error for three different stents.

The maximum alowed error corresponds to 3 pixels distance with the 5X lens. To meet this constraint, roller excentricity needs to be less than 5µm in case of a coronary stent of 1.5mm

As regards to the error in Z direction, we have determined numerically that the maxima is found at rotation angle φ=π and the minima is at φ=0. Therefore, we define the maximum Z error as :

$$PV_Z = N_Z\big|_{\varphi=\pi} - N_Z\big|_{\varphi=0} \quad \textbf{(22)}$$

In Figure 20 the maximum Z error as a function of excentricity error is shown, for three different stent diameters. This error now decreases with the stent diameter, due to the roller contact point slope decreases.

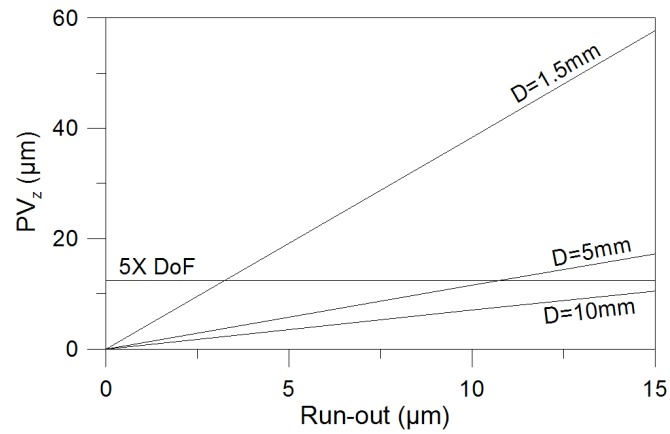

Fig. 20. Excentricity Z projection error for three different stents.

As in Figure 17, the maximum allowed limit is the depth of field of the 5X lens as a reference. To keep the stent apex always in focus, the maximum allowed excentricity error is around 3µm. This constraint is extremely tight for small diameters due to not only the vertical roller shift, but also the lateral roller contribution, which causes the stent to move vertically as well.

The excentricity influence taking a stationary roller have been calculated. Taking into account that both rollers can have a specific excentricity, maximum allowed error will be the half of the ones stated above.

6. CONCLUSIONS

In this paper, a new system for stent inspection is proposed. We have presented a novel lighting arrangement together with a high precision rotational stage that allows us to acquire high resolution images in a line-scan manner, which needed an specific, custom calibration specimen to evaluate its performance and calibrate its accuracy.

We have revealed that the critical dimension measurements with a conventional microscope differs from the real dimensions that can be obtained by our unrolled approach. We have also proposed the geometrical relationship between both measurements.

As regards to calibration, we have designed and manufactured a novel calibration specimen that allows us to calibrate the magnification of the system in the unrolled direction.

Finally, construction errors and tolerance limits have been identified to be able to perform said high resolution images without defocus and to meet critical dimension measurements requirements.

References

1. D. Freifeld, *Repetitive inspection system with intelligent tools*, US Patent 6,606,403 (2003).

2. E. Maehringer-Kunz, et al., *Automatic inspection device for stents, and method of automatic inspection*, PCT/EP2006/065814 (2006).A
3. I. Ibraheem, A. Binder, *An automated inspection system for stents*. The International Journal of Advanced Manufacturing Technology A **47**, 945-951 (2009).
4. F. Laguarta, et al., *Device and method for optically inspecting and analysing stent-like objects*, WO2015/096874 (2015).